Simulation of the Loading Parameter in Organic Nonlinear Optical Materials†

R. D. Nielsen, H. L. Rommel, and B. H. Robinson*

Department of Chemistry, University of Washington, Seattle, Washington 98195

Received: September 30, 2003; In Final Form: December 12, 2003

The optical properties of organic chromophores, in the class of nonlinear optical molecules, have improved dramatically. These chromophores have large hyperpolarizability and large permanent dipole moments, in excess of 10 D. When these molecules are mixed with a host polymer at high chromophore density and processed using an aligning electric poling field, the resulting material does not have the electro-optic (EO) response promised by the individual molecules. We have used equilibrium statistical mechanics, and Monte Carlo (MC) methods in a lattice-based model, to investigate how the molecular properties translate into the EO response of the material. We compare our MC results with a previously developed analytic theory and find good agreement when certain assumptions about the analytic theory are made. By use of the MC methods to compute order parameters for chromophores at high density on a lattice in the presence of an external uniform poling field, we find that greater order and hence greater EO performance can be obtained by adjusting the geometry of the lattice. This suggests that modifications to existing chromophores could lead to improvements in the EO properties of the materials. We compare with other lattice and mean field models. In our lattice model, we find no ferroelectric phase transition.

I. Introduction

There is intense current interest in developing nonlinear optical (NLO) materials that couple applied electric fields to optical transmission.[1−3] Electro-optic (EO) modulators are devices that shift the index of refraction of an optical wave through the application of a static or low-frequency electric field.[4] EO modulators have wide applications in signal processing and data transmission. EO transducers are necessary components to interface optical and electrical networks. Optical switching and optical phase and amplitude encoding have applications ranging from radar detection to optical computing.[5] There has been a recent movement in the design of NLO materials away from reliance on solid-state inorganic crystals as EO materials. Organic chromophores embedded in amorphous guest−host polymers have emerged as novel NLO materials.[6,7] The reasons for this shift are manifold. Some of the major factors are ease of fabrication, better index of refraction matching between active and passive waveguides, and superior EO properties of organic NLO materials. The fabrication techniques in conventional solid-state devices appear to have reached a saturation point where large factors of improvement in crystal quality and EO activity seem to be obtainable only at the cost of a concomitant increase in complexity of fabrication. The relative ease of fabrication with organic chromophores is an attractive feature of these materials. There is still much room for optimization of organic NLO materials both in molecular design and fabrication. We address a major bottleneck in the optimization of organic NLO EO activity.

Organic NLO materials are fabricated from organic molecules that have large molecular second-order hyperpolarizabilities (β).[2,8] To ensure a maximum *macroscopic* hyperpolarizability, the chromophores must be organized with a macroscopic axis of acentric order. Only with a large degree of acentric order can all of the individual molecular hyperpolarizabilities act in concert to produce the desired large macroscopic EO effect. Alignment of NLO chromophores usually takes advantage of the large electric dipole moment μ that accompanies large β molecules. The principal axis of the dipole moment coincides to a good approximation with the principal axis of the hyperpolarizability tensor.[9] The NLO materials can be fabricated by spin casting the organic materials in a guest polymer (for example, polymethyl methacrylate (PMMA) and amorphous polycarbonate (APC)). The chromophore/polymer system is heated above the glass transition temperature of the composite and is subject to a large applied electric field (poling field). The poling field aligns the organic molecules because of the field−dipole interaction energy $-\vec{\mu}\vec{E}_p = -|\vec{\mu}||\vec{E}_p| \cos(\theta)$. Once molecular alignment is imposed, the polymer is cooled to kinetically trap the ordered NLO molecules in the polymer matrix. The efficiency of the poling process in NLO fabrication is the focus of this paper. The average value of the projection of the molecular dipole axis onto the direction of the poling field is a measure of the efficiency of alignment $\langle\cos(\theta)\rangle$. The degree of acentic order is also reflected in the average $\langle\cos^3(\theta)\rangle$. The latter quantity is preferable as a measure of alignment because the shift in index of refraction of light propagating through the NLO material that is induced by an externally applied DC field is proportional to $\langle\cos^3(\theta)\rangle$ when the polarization of the incident light and induced polarization of the material are both the same direction as the DC field. The cube of $\cos(\theta)$ enters in this configuration of the fields because the polarization of incident light, applied field, and induced polarization all share the same polarization axis relative to an individual molecular β axis. The shift in index of refraction n_{zz} for a given applied DC field E_z is conventionally defined as $\Delta n_{zz} = -{}^1/_2 n_{zz}{}^3 r_{zzz} E_z$, where the proportionality constant (EO

† Part of the special issue "Alvin L. Kwiram Festschrift".

* Author to whom correspondence may be addressed. E-mail: robinson@chem.washington.edu.

10.1021/jp0369239 CCC: $27.50
Published on Web 01/27/2004

coefficient) is[10−12]

$$r_{zzz} \equiv r_{33} = -2\frac{F^{\text{local}}\beta_{zzz}(-\omega,\omega,0)}{n_{zz}^{4}} N\langle\cos^3\theta\rangle$$

The frequency-dependent hyperpolarizability $\beta_{zzz}(-\omega,\omega,0)$ and local field factor F^{local} are important to the EO effect but are not discussed here. The density of NLO chromophores N can be combined with the geometric factor to define the loading parameter $\text{LP} = N\langle\cos^3\theta\rangle$. The loading parameter must be optimized to obtain the greatest available EO activity for a given chromophore. The paper is divided into two sections. In section II, two analytic approaches are discussed that allow the statistical partition function to be calculated. First, a recently developed model that allows for the loading parameter to be calculated as a function of molecular density, dipole moment, and temperature is reviewed. A second model that pertains to only one-dimensional chains of dipoles is presented. The analytic approaches to the statistical mechanics of chromophore alignment are provided because they enhance understanding of numerical Monte Carlo (MC) simulations discussed in section III.

II. Analytic theory

The calculation of the loading parameter is straightforward in the case of dilute concentrations of chromophores in the applied poling field. When the chromophores are sufficiently dilute, the chromophore−chromophore dipole−dipole interactions can be neglected. The Langevin theory of dilute magnetic dipoles can be carried over immediately to the electric dipoles of the chromophores in the poling field. In this case, the classical partition function for a single chromophore using only the dipole-field interaction energy is[4]

$$G(f) = \frac{\sinh(f)}{f}$$

where f is the strength of the dipole−field interaction defined as

$$f = \frac{E_{\text{p}}\mu}{\epsilon kT}$$

Averages are calculated from the partition function as a generator

$$\langle\cos^n(\theta)\rangle = \frac{1}{G(z)}\frac{\partial^n G(z)}{\partial^n z}\bigg|_{z=f}$$

For example

$$\text{LP} = N\langle\cos^3(\theta)\rangle = NL_3(f) \approx N\left\{\frac{1}{5}\frac{E_{\text{p}}\mu}{\epsilon kT} + O(f^3)\right\}$$

where $L_3(f)$ is the third-order Langevin function.[4,11] A linear dependence of the loading parameter on density is observed in dilute systems experimentally.[2] Empirically, the loading parameter reaches a maximum as the density increases and diminishes as the chromophore density is further increased. This phenomenon has been attributed to dipole−dipole interactions of the chromophores at high density.[2]

Recently, the simple Langevin partition function has been modified to model the effect of dipole−dipole interaction. The method of modification follows upon the seminal work of Piekara.[13] In the Piekara approach, the effect of the many-body molecular dipole interaction is accounted for as an effective single-particle field acting on a representative chromophore. Figure 1, left, shows a pictorial representation of Piekara's model. It is assumed that a typical chromophore is embedded in a local field that is comprised of the surrounding dipoles in its immediate neighborhood. The local field is assumed, for simplicity, to have a single axis of symmetry. The local field is envisioned as a locally ordered domain (a local crystallite field (LCF)). The entire material is modeled as a collection of crystallite domains with uniformly random macroscopic orientations. The approach is not self-consistent in the sense that the LCF is constructed of the very dipoles that are the subject of the statistical calculation. The LCF is itself statistical in nature. The local field assumes the form $W\cos(\gamma)$, as a first-order expansion of local field−dipole interaction in spherical harmonics (where γ is the relative angle of the axis of symmetry of the LCF and the representative chromophore dipole moment). W is the unspecified strength of the interaction of the dipole with the LCF.

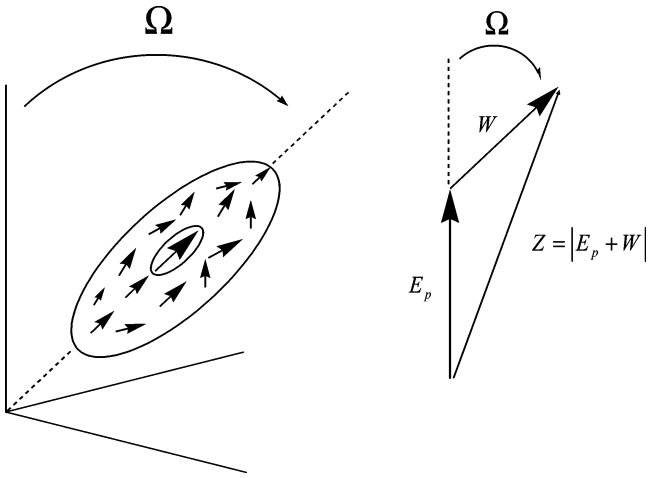

Figure 1. Schematic of the Piekara local crystallite field. The crystallite (left) has the macroscopic orientation Ω with respect to the poling field E_{p}. The local crystallite field W adds vectorially to the external poling field E_{p} (see eq 1).

With this local field, the argument of the Langevin partition function is replaced by

$$z = (f^2 + w^2 + 2fw\cos(\Omega))^{1/2} \qquad (1)$$

where $w = W\mu/kT$ and Ω is the macroscopic orientation of a particular LCF.[4,14] A physical interpretation of this substitution is that the magnitude of the external poling field−dipole interaction of the Langevin theory is replaced by the magnitude of the vector sum of the poling field and LCF interactions (see Figure 1, right). The averages of interest are now calculated as

$$\langle\cos^n(\theta)\rangle = \frac{1}{2}\int_{\cos(\Omega)=-1}^{1}\frac{1}{G(z)}\frac{\partial^n G(z)}{\partial^n f}d\cos\Omega \qquad (2)$$

The integral represents the statistical average over all of the uniformly distributed crystallite domains. The LCF competes with the external poling field directly. When the LCF dominates (as might be expected at high chromophore densities where dipole−dipole interactions are strong), the average dipole orientation tracks the orientation of the crystallite field and uniform averaging of the dipole orientation is produced via the uniform average over LCF orientations. When the LCF is

removed by setting w to zero, eq 2 reduces to the Langevin partition function.

While a sufficiently strong monotonically increasing dependence of W on density N is sufficient to qualitatively account for the saturation of loading parameter with increasing density, a specific form of W is useful for quantitative comparison. A dependence of W on dipole moment and temperature is expected given the statistical nature of W as an effective field in addition to the density dependence. It may be argued that the problem of dipole−dipole interactions has not been solved by the Piekara approach but has merely been sequestered in the ambiguous dependence of W on molecular parameters and unknown statistical dependence upon temperature. On the other hand, the Piekara formulation provides a simple analytic framework in which a guess at the form of W may be tested easily and used to model the saturation behavior of the loading parameter. We have developed a particular parametrization of W by considering the magnitude of dipole−dipole interactions in the absence of a poling field.[4,13] This first pass at self-consistency gives

$$w = \frac{W\mu}{kT} = s\left(\frac{N\mu^2}{kT}\right)^2 \tag{3}$$

where s is an adjustable scaling constant presumed to be independent of density, temperature, and dipole moment but may depend on the local geometric arrangement of dipole centers.

The following relation, derived using the form of W (eq 3) substituted into eq 2, determines the value of density N, which the loading parameter is maximal, N_{max}

$$w_{max} = s\left(\frac{\mu^2 N_{max}}{kT}\right)^2 \approx 1.9139... + O\left(\frac{E_p\mu}{\epsilon kT}\right)^2 \tag{4}$$

We remark that the dependence of w_{max} on $f = E_p\mu/\epsilon kT$ is well approximated by a simple square root function that is described elsewhere.[4] The expansion to first order in f given by eq 4 is reasonable because of the low experimentally obtainable values of the poling field. Equation 4 constitutes a simple "rule of thumb" that predicts a strong inverse relation between the dipole moment and the density at maximum of the loading parameter. From eq 4, it follows that the maximum value of the loading parameter can be written as a function of E_p, μ, and T (see discussion).

Section III shows MC simulations of dipoles in a poling field. The statistics of dipole−dipole correlation are compared with the Boltzmann distribution of relative angles expected from the LCF interaction energy $W\cos(\gamma)$. A range of densities, dipole values, and temperatures are used to compare the form of W with the results of MC simulations.

One of our goals is to compare MC dipole ordering obtained with different lattice arrangements of chromophores. One such lattice arrangement is a distorted simple cubic lattice, where one dimension is compressed and the orthogonal dimensions are expanded to keep constant density, a tetragonal lattice. For sufficient distortion, that lattice resembles a set of one-dimensional columns. Therefore, an ideal case we wish to consider is that of a single column comprised of many dipoles. If we consider only nearest-neighbor dipole−dipole interactions, in a single one-dimensional line of dipoles and in the presence of the poling field (pointing in the direction of the column), the partition function may be found almost analytically. The averages can then be generated, and compared to the MC simulations on distorted lattices, to see if the behavior of the distorted lattice resembles independent one-dimensional columns of dipoles. We use the transfer matrix method.[15] $T_{1,2}$ is a matrix representing all possible orientations of a dipole and its nearest neighbor (separated by the distance r_z)

$$T_{1,2} = \exp^{f(u_1+u_2)/2+2d(u_1\cdot u_2)} I_o(dz_{1,2}) \tag{5}$$

where $d = \mu^2/r_z^3 k_B T$, $z_{1,2} = ((1-u_1^2)(1-u_2^2))^{1/2}$, and $u_1 = \cos(\theta_1)$. To cast $T_{1,2}$ into a matrix form, a uniform grid of the angle space, in units of $\cos\theta$, is used. This assumes re-entrant boundary conditions on the major angle. The minor angle can be integrated, resulting in the Bessel function, $I_o(dz_{1,2})$. The partition function is

$$G(f,d) = tr\{T_{1,2}{}^M\} = \sum_i \lambda_i^M$$

for a system of M dipoles, where λ_i are the eigenvalues of the $T_{1,2}$ matrix. The averages (order parameters) can be computed from the partition function.

III. Monte Carlo Simulations

Simulations require a definition of the total dipole−dipole energy for the entire system. The total electrostatic potential energy, U, must be written in terms of the position and orientation of each dipole. The set of interacting dipoles in a poling field is the sum of the interaction energies over all dipoles with the field and all dipole−dipole interactions.[16] The electrostatic potential energy is

$$U = \sum_i \left\{ \frac{\vec{\mu}_i \vec{E}_p}{\epsilon} + \frac{\mu^2}{r_z^3} \sum_j \frac{\hat{\mu}_i \hat{\mu}_j - 3(\hat{\mu}_i \hat{d}_{ij})(\hat{d}_{ij}\hat{\mu}_j)}{d_{ij}^3} \right\}$$

$$\frac{U}{k_B T} = f \sum_i \hat{\mu}_i \hat{E} + d \sum_{i,j} \frac{\hat{\mu}_i \hat{\mu}_j - 3(\hat{\mu}_i \hat{d}_{ij})(\hat{d}_{ij}\hat{\mu}_j)}{d_{ij}^3}$$

μ is the magnitude of the chromophore dipole, E_p is the applied poling field, and ϵ is the dielectric constant of the host. The strength of the electrostatic energy then is controlled by two dimensionless parameters, $f = |\mu||E_p|/\epsilon k_B T$ and $d = \mu^2/r_z^3 k_B T$. Here $d_{ij} = r_{ij}/r_z$ is the distance between dipoles i and j relative to the nearest-neighbor dipole distance r_z. The chromophore density, for a uniform lattice, is $N = 1/r_z^3$. Each quantity with a "hat" over it is a unit vector of that quantity.

MC simulations of simple cubic and body-centered cubic lattices of point dipoles were implemented using periodic boundary conditions as described elsewhere.[2,4,10] In the present calculations, the sum over the dipole−dipole interactions is restricted using the minimum image convention.[11,17] Because the chromophores are constrained to reside on a lattice, they cannot act like a true liquid; however, the chromophores are allowed to adopt completely arbitrary orientations.

For the case of a simple cubic lattice, the dipoles were placed M by M by M, where values of M from 10 through 13 were examined. We also considered stretched, or tetragonal, lattices, in which the distance between nearest neighbors in the X, Y, and Z directions were allowed to be different. To gain an understanding of the effective local field experienced by a representative dipole, MC simulations of a dipole lattice in the absence of a poling field were explored first. The statistical orientation of a given dipole relative to the orientation of its neighbors was determined by a histogram of the projections of each dipole in the lattice onto its first shell of neighbors. This gives the distribution of the relative angle between neighboring dipoles, $\cos(\gamma)$. Figure 2 shows a set of histograms, each

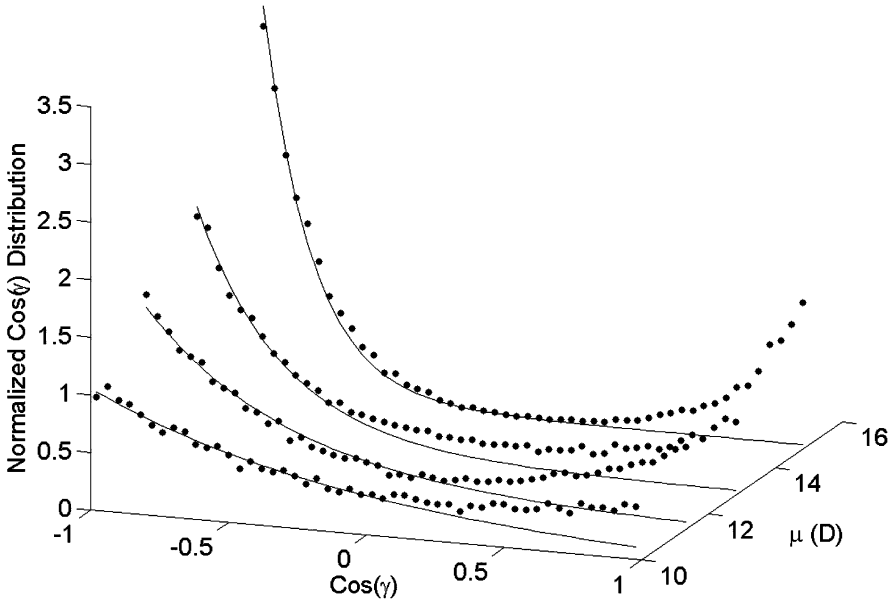

Figure 2. Normalized nearest-neighbor distribution as a function of the relative angle cos(γ) between neighbors for $N = 10^{21}$ molecules/cc and $T = 373$ K. The distributions are composed from a histogram of nearest-neighbor angles compiled for all lattice sites. The distributions are plotted for a set of dipole moments (shown on the *Y* axis in Debye). Superimposed are the fits to the single-exponential distribution using the form of the local field function in the text.

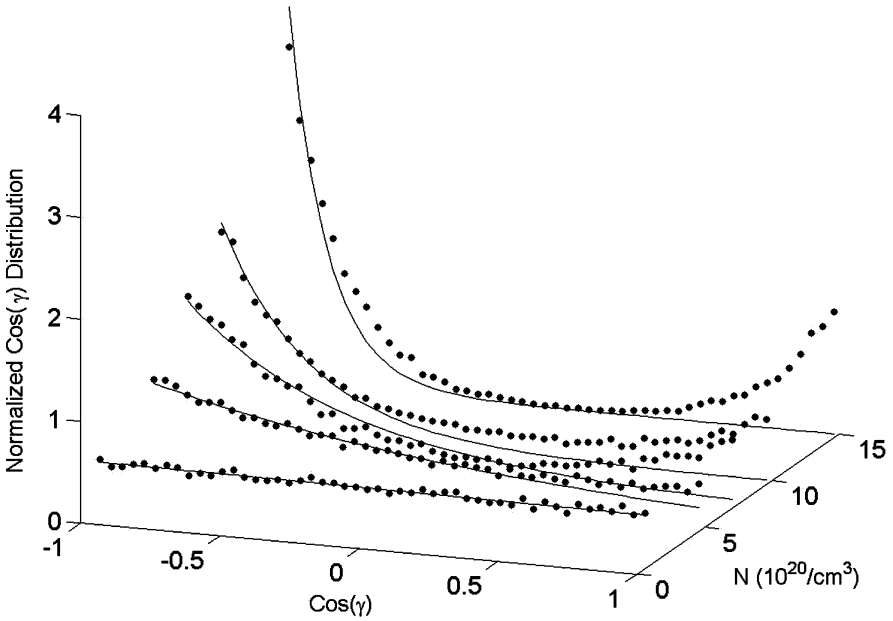

Figure 3. Normalized nearest-neighbor distribution as a function of the relative angle cos(γ) between neighbors for $\mu = 13$ D and $T = 373$ K. The distributions are composed from a histogram of nearest-neighbor angles compiled for all lattice sites. The distributions are plotted for a set of densities (shown on the *Y* axis in molecules/cc). Superimposed are the fits to the single-exponential distribution using the form of the local field function in the text.

corresponding to a MC simulation of chromophores with a different dipole moment (dots). All simulations were at a fixed chromophore density of $N = 10^{21}$ molecules/cc and fixed temperature of 373 K. Figure 3 shows the result of MC simulations with varying density (*N*) for a fixed dipole moment and temperature. Figure 4 shows results for different temperatures fixing the density and dipole moment. All cases show that the majority of neighbors surrounding a given dipole have opposing orientations. A second population of neighboring dipole orientations is evident on the rhs. These are aligned with the central dipole. Both subpopulations have a distribution that appears to be exponential as a function of cos(γ). The analytic theory introduced in section II postulated a simple interaction between a given dipole and its immediate environment. The interaction energy was parametrized by a cosine projection of the center dipole onto a local axis of symmetry. The presence of a second distribution in the MC histograms runs counter to the interpretation of the Piekara field. The dependence of the Piekara field *W* on density, dipole moment, and temperature is tested by focusing on the most prominent (opposing nearest neighbor, cos $\gamma < 0$) distribution. Figures 2−4 show an overlay of the MC distributions with the function

$$P(\cos(\gamma)) = A\, e^{-0.3(N\mu^2/kT)^2 \cos(\gamma)} \tag{6}$$

The prefactor *A* was adjusted so that the Piekara distribution function fit the opposing nearest-neighbor distribution. The arbitrary scale factor *s* in the Piekara field was set to 0.3. The

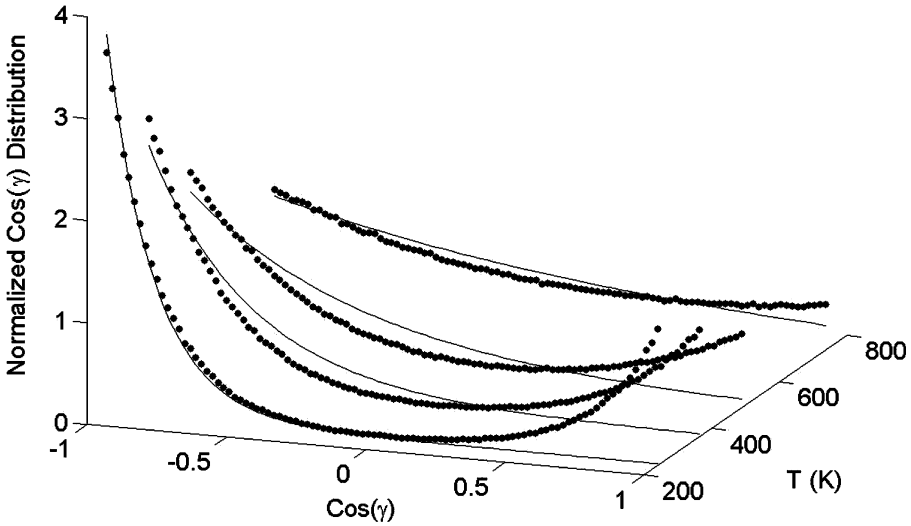

Figure 4. Normalized nearest-neighbor distribution as a function of the relative angle cos(γ) between neighbors for $N = 10^{21}$ molecules/cc and $\mu = 13$ D. The distributions are composed from a histogram of nearest-neighbor angles compiled for all lattice sites. The distributions are plotted for a set of temperatures (shown on the *Y* axis in Kelvin). Superimposed are the fits to the single-exponential distribution using the form of the local field function in the text.

density, dipole moment, and temperature dependence of the Piekara distribution tracks the behavior of the most prominent distribution in the MC simulations of Figures 2−4. Further optimization of the Piekara energy *w* by variation of the pre-exponential factor *A* and the power law dependence of (μ^2N/k_BT) for each set shown in Figures 2−4 using nonlinear least-squares optimization illustrated the assumption that *w* is proportional to the square of μ^2N/k_BT is better than any other integer or half integer power (not shown).

The histograms generated from the MC calculations are better fit to the functional form

$$P(\gamma) = A\{\exp^{-0.3w\cos\gamma} + B\exp^{0.3w\cos\gamma}\}$$

where *B* is $\sim{}^1/_3$ and is independent of μ and N but does depend on the lattice geometry. The use of body-centered cubic (bcc) lattice geometry gave nearly identical results, and *B* increased to around $^1/_2$. Neglecting the increasing part of the distribution (i.e., setting $B = 0$) makes Piekara's conjecture nearly quantitative.

The statistics described so far pertain to nearest-neighbor angular distributions. A clearer picture of the behavior of the dipolar lattice is obtained by looking at the statistics of projections onto the external (lattice) *x*, *y*, and *z* axes. Further analysis of the MC results showed that long-range statistical order exists in the form of alternating planes of dipole polarization, in the case of a simple cubic lattice. Figure 5 shows one particular state that is indicative of those found for a simple cubic lattice in the course of a long MC trajectory. In the case shown, the *x* axis is the unique axis along which polarization on a plane-by-plane basis is found.

Examination of the statistics within individual *xy* planes revealed a net Boltzmann weighted polarization in the direction of the *x* axis. The net direction of this polarization alternated between adjacent *xy* planes, either with or against the positive *x* axis. Because adjacent planes have opposite polarization, the lattice has no net ferroelectric order. The polarization (in a plane by plane sense) may be found along the *X*, *Y*, and *Z* axes with equal probability over a sufficiently long MC run; typically, 10^5 MC cycles are sufficient to exhibit all three states multiple times. The set of *xy* planes that exhibit alternating net polarization from plane to plane (as in Figure 5) are denoted as the *xy*

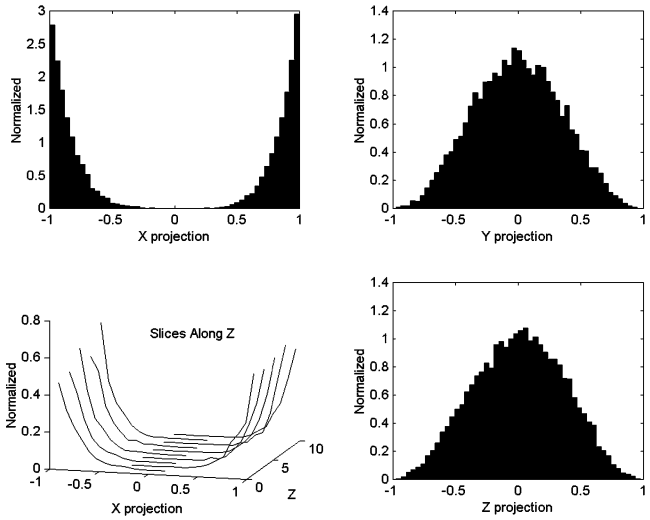

Figure 5. The *X*, *Y*, and *Z* projections of the dipoles in a 10 × 10 × 10 simple cubic lattice plotted as histograms for the last fifty cycles of an equilibrated MC trajectory (1 × 10^5 MC cycles). The unique histogram found for the *X* projection was broken up into separate plane-by-plane statistics as a histogram of the *X* projection for individual slices along *Z* (*xy* planes), lower left figure.

states. Similarly there are *xz* and *yz* states. Such polarization is statistical and long range, as it persists from one side of the lattice to the other. In the absence of a poling field, all three choices of plane polarization are encountered with equal probability and show the same stability as a function of MC cycles. Figure 6, left, shows a cartoon of a unit cell from the lattice in the *xy* state. The polarizations are exaggerated and are not drawn to reflect equilibrium statistics but are meant to represent the net geometry. This picture of the unit cell explains the nearest-neighbor statistics presented above. Namely, the predominant nearest-neighbor dipole orientation, consisting of opposing dipoles, is comprised of the top and bottom planes. The minor component of the nearest-neighbor distribution comprises the dipoles in the center plane.

In the presence of a poling field, oriented along *Z*, a superposition of paraelectric ordering due to the poling field and anti-ferroelectric statistical polarization is found. The presence of the poling field breaks symmetry and disrupts the

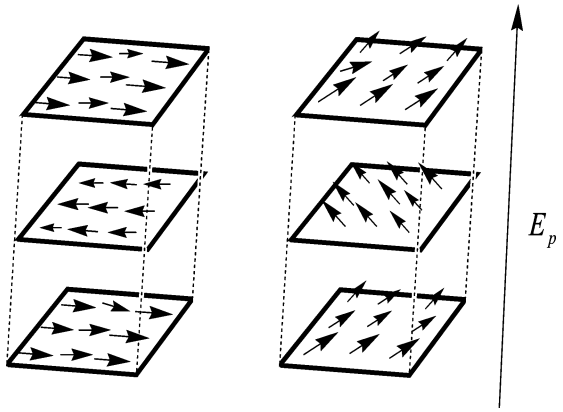

Figure 6. A schematic representation of the *xy* state defined in the text and Figure 5. The polarizations are exaggerated and are not drawn to reflect equilibrium statistics. The left figure is in the absence of an external field. The right figure shows the effect on the *xy* state of a poling field oriented along *z*.

probability with which the three different polarizations of long-range order, discussed above, occur. The lowest energy states found in the course of a MC run, with a poling field along *Z*, are the states such that the long-range order described above arises from alternating polarization in the *xy* plane (see Figure 6, right). In these states, the polarization of the *xy* states directly compete with the poling field for order in the *z* direction by presenting a tendency to localize dipole orientation in the *xy* planes.

Figure 7 shows the average value of $\langle\cos^3(\theta)\rangle_{MC}$ for a typical MC run of 2×10^5 cycles in the presence of a strong poling field (600 V/μm), dipole moment $\mu = 13$ D, and density $N = 7.5 \times 10^{20}$ molecules/cc. The initial configuration of dipole orientations was random. After $\sim 10^4$ cycles, the MC trajectory stabilized to a predictable pattern, closely approximating the equilibrium conditions. There is a dominant state characterized by $\langle\cos^3(\theta)\rangle_{MC} \approx 0.16$ and less populated (higher-energy) states between 0.22 and 0.26. All of these states differ by less than 0.1 kT per dipole. The projection of dipole orientations along the direction of the poling field is displayed as a histogram over the lattice for representatives of two of these states (see Figure 7, right). The lower-energy (dominant) state corresponds to the cartoon in Figure 6, right, and is the *xy* states described above superposed with the effect of the poling field. The higher-energy states are the result of the *yz* or *xz* configurations described above superposed with the effect of the poling field.

Figure 8 shows the value of the loading parameter as a function of density. The discrete points are MC results, where the value of $\langle\cos^3(\theta)\rangle_{MC}$ has been selected from the lowest-energy configuration encountered in the course of the MC trajectory at each density. For reference, the distribution of $\langle\cos^3(\theta)\rangle_{MC}$ at the $N = 7.5 \times 10^{20}$ molecules/cc was compiled over the entire MC trajectory (neglecting the first 10^4 cycles). The loading parameter calculated from the MC statistics is compared with the results from the analytic theory described in section II. The scale factor, *s*, was chosen to be $^7/_4$ to give agreement between the prediction of the loading parameter from the analytic theory and the results of the MC calculations. That a scaling value of $^7/_4$ was necessary for agreement would appear at first to contradict the scaling value of 0.3 found in Figures 2−4 where the nearest-neighbor distributions from MC were compared to local field function of analytic theory (see eq 6). We suggest that the larger scale factor is needed to correct the analytic theory for stability of long-range order in the dipole lattice. The *w* factor, which models the environment of a chromophore, is in fact comprised of the cooperative effects of neighboring chromophores and is part of the sampling statistics of the MC calculations. The interactions generating a cohesive force within the embedded crystallite, as seen in the MC calculations, are long range and are not contained in the simpler analytic theory that inherently models local order. The MC calculations have shown, however, that to a good approximation the form of *w* given above (see eq 3) captures the local environment and the dependence of the local interparticle dipole distribution on μ, *N*, and *T*.

One method of potentially improving the loading would be to vary the lattice geometry. Therefore we explored the effects

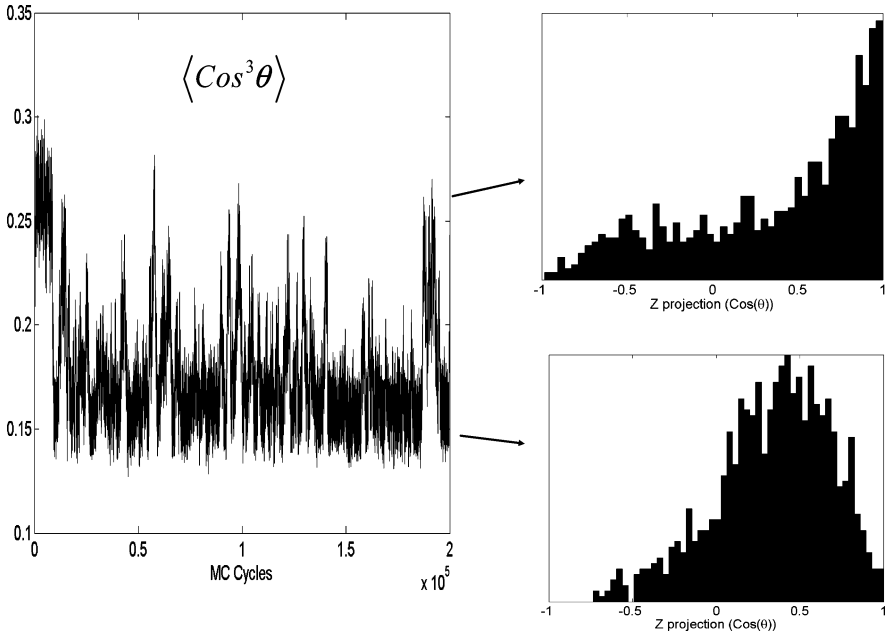

Figure 7. Left: $\langle\cos^3(\theta)\rangle_{MC}$ for a MC run of 2×10^5 cycles in the presence of a strong poling field (600 $V/\mu m$), dipole moment $\mu = 13$ D, and density $N = 7.5 \times 10^{20}$ molecules/cc. The initial configuration of dipole orientations was random. Right: Histograms over all lattice sites of the *z* projection of dipole orientation for two representatives taken out of the MC trajectory which correspond to the low-energy (*xy*) (bottom) and high-energy states (*yz*) (top). The geometry of the state in the bottom right figure is represented schematically in Figure 6, right.

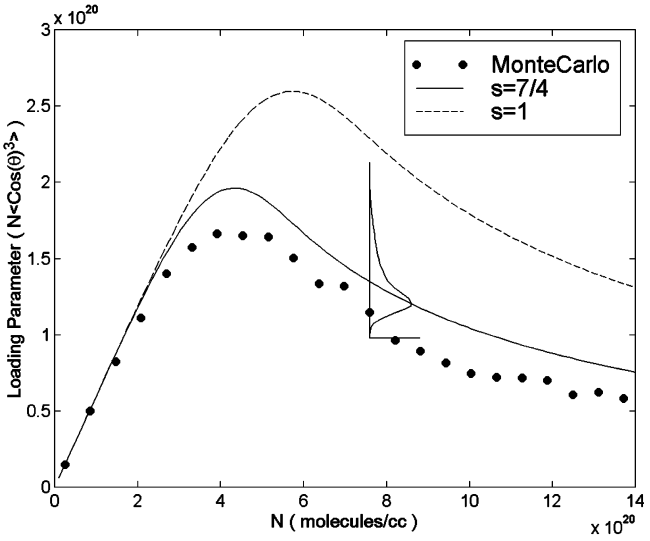

Figure 8. Plot of the loading parameter as a function of chromophore density, N, with μ =13 D and a poling field of 600 V/μm, corresponding to $f \approx 5$. The lines are calculated according to eq 2, with a scaling on w of $s = 1$ (dashed line) and $s = 1.75$ (solid line). The filed circles are results from MC calculations, for the lowest energy configurations (xy plane states), as a function of density N. The inset is the histogram distribution of loading parameters found in the course of MC run at a density of $N = 7.5 \times 10^{20}$ molecules/cc (see Figure 7).

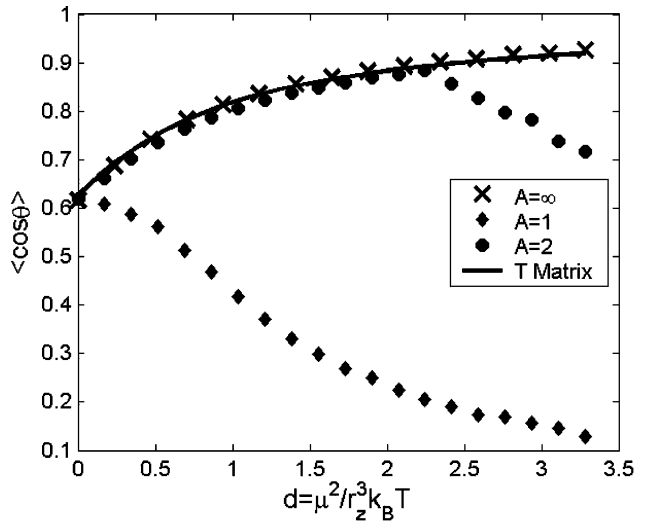

Figure 9. The average-order parameter, $\langle \cos\theta \rangle$, as a function of the strength of the nearest-neighbor interaction parameter (along Z), $d = \mu^2/r_z^3 k_B T$, for three distinct cases, $A = 1$, 2, ∞, calculated by MC methods. Here the dipole moment was fixed at $\mu = 13$ D; the poling field strength parameter was fixed to $f \approx 2.5$, which corresponds to a field of $E_p/\epsilon = 300$ V/μm and $T = 373$ K. ♦, $A = 1$; ●, $A = 2$; and ×, $A = \infty$; the solid line was calculated using the transfer matrix method of eq 5.

of changing the distance between chromophores in the XY plane relative to the distance between chromophores in the Z direction (which is the direction of the external poling field). The distance between chromophores in the Z direction is r_z. This distortion is parametrized by an aspect ratio, A. For example, when $A = 2$, the distance between nearest dipoles in the XY plane is twice that of the distance between nearest-neighbor dipoles on the Z direction.

Figure 9 shows the average order parameter, $\langle \cos\theta \rangle$, as a function of the strength of the nearest-neighbor interaction parameter, $d = \mu^2/r_z^3 k_B T$, for three different cases: the simple cubic lattice with $A = 1$, the distorted cubic (or tetragonal) lattice with $A = 2$, and the extreme case of a single column of dipoles, denoted $A = \infty$. To test that the MC calculations were finding all equilibrium distributions, we compared the order parameters for the $A = \infty$ case with order parameters obtained from the transfer matrix method. Only nearest-neighbor dipolar interactions were retained in the $A = \infty$ calculation (shown in Figure 9). However, calculations including next-nearest neighbors were also carried out, with similar results (not shown). When the aspect ratio is $A \geq 2$, the interactions along Z dominate. To simulate these interactions with a MC calculation, longer chains are used to give a larger distribution of equilibrium structures within a given set of MC cycles. All computations, in which $A = 1$ or 2, used a 10 by 10 by 10 array of 1000 dipoles. In each case, the system was initialized with random orientations, allowed to run for 10 000 MC cycles, and the order parameters were obtained by averaging the order from the last 5 000 cycles. This was performed 100 times and the final result averaged.

For the one-dimensional lattice, $A = \infty$, the solid line is the analytic result using the transfer matrix method of eq 5, and the numerical simulations (shown as Xs) were done using 10 dipoles in a line along the direction of the field. The order parameters were obtained using the same averaging protocol. MC calculations for systems of 100 and 1000 dipoles yielded nearly identical results (data not shown).

Nearest-neighbor statistics of the relative dipole orientations for the $A = 2$ lattice of Figure 9 show that the dipoles organize statistically into columnar order. The columnar order is oriented either with or against the external poling field axis. Within a given column of statistical order, the cosine projection of the individual dipoles onto the unique columnar axis exceeds 0.85 for all density points in Figure 9. The columnar order that is found when $A = 2$ is in contrast to the plane-by-plane statistical order that was observed in the $A = 1$ case (see Figure 5). The average order as a function of dipole separation for the $A = 2$ case (●) agrees with the analytic theory for a single column of dipoles (—) over a large density range and reflects the columnar nature of the dipole statistics in the $A = 2$ case. When the poling field is turned off in the $A = 2$ case, the same columnar order arises internally, but the net number of dipolar columns aligned or opposed to the external axis are equal and give net antiferroelectric order of the lattice (data not shown).

Figure 10 shows the loading parameter as a function of the chromophore number density, N, for the case where the aspect ratio is varied, $A = 1$ or 2 (● and ♦, respectively). The calculations were performed as described above (see Figure 9 text). The distance between chromophores is 10 Å for the uniform ($A = 1$) case when the number density is 10×10^{20}/cc. For the distorted lattice ($A = 2$), the point where the distance between neighboring chromophores on z is 10 Å occurs at 2.5×10^{20}/cc. This point is marked with an arrow. The errors are drawn one standard deviation about the mean and reflect the presence of nearly equal energy states that differ in their statistical dipole geometries (see the above description of Figure 8). The maximum loading parameter for the distorted case is over 2-fold larger than for the uniform lattice case. Moreover, the density dependence of the loading parameter levels off after an initial rise. The analytic theory from eq 2 with $s = {}^7/_4$ (see Figure 5) is plotted in Figure 10 for comparison.

Discussion

The analytic theory presented in the first section is a simplified approach to the complex problem of many-body dipolar interaction. It is a mean-field approach that does not contain a mechanism for self-consistency of the local single-

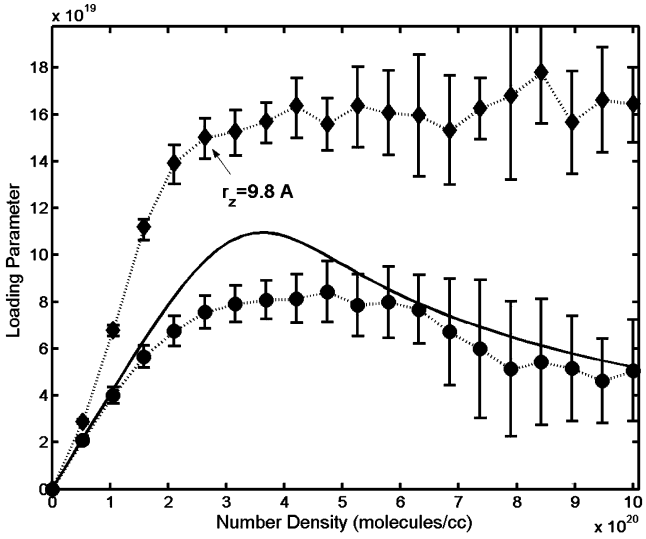

Figure 10. The loading parameter is plotted as a function of chromophore number density (in units of molecules/cc) for the uniform lattice, $A = 1$ (●), and the tetragonal lattice, $A = 2$ (♦). The loading parameter for the tetragonal lattice is 2-fold larger than for the uniform lattice after a minimal density of around 2×10^{20}/cc and does not show any falloff with increased density. Also shown is the analytic theory (solid line) of eq 2 for the uniform lattice case, with $s = 1.75$. All other parameters are the same as Figure 9.

particle mean field with the derived value of dipole polarization. The mean field is assumed to arise from a local dipole order. Despite these restrictions, the analytic approach provides a simple way to visualize and model the competition of dipole−dipole forces, which cause anti-ferroelectric ordering of dipoles, in the presence of an orienting external field. The simple parametrization of the local field presented above in eq 3 leads to a potentially important prediction: The simple analytic theory and the numerical MC results illustrate the experimentally observed conundrum that larger dipole moments do not necessarily lead to greater loading. The maximum loading can actually be reduced when the dipole moments become large. Additionally, and more obviously, there is a tradeoff of order with chromophore density.

The maximum of the EO effect occurs where the loading parameter is maximal. The dependence of the loading parameter maximum on poling field and dipole moment is most easily seen in the low poling field limit where $E_p\mu/\epsilon kT \ll 1$. The density of chromophores at which the loading parameter is maximal varies inversely with the square of the dipole moment (eq 4). Within the low poling field regime, $LP_{max} = N_{max} \langle \cos^3 \theta \rangle \propto E_p/\mu$, as may be seen from expansion of $\langle \cos^3 \theta \rangle$ in powers of the poling field.[10,11] The net result is that, according to the analytic theory, increasing the value of the dipole moment does not improve the maximum value of the loading parameter. According to the analytic theory, increasing the density of chromophores will always offset the reduction in net dipole ordering that is incurred as a result of lowering the dipole moment. Physically, however, the density may not be increased indefinitely. The dipole moment should, therefore, be tailored to the maximum attainable density according to eq 4 to obtain the best loading parameter. In interpreting the latter prediction, it should be realized that the results discussed here only pertain to electrostatics; steric effects were not included. At high densities, steric interactions become competitive with electrostatics. The analytic theory discussed here has been modified to include steric constraints, which were required to achieve quantitative agreement with experimental data.[2,4,10] With the inclusion of steric constraints, detailed calculations are needed to determine the optimum dipole moment within the constraints dictated by the molecular architecture. It should also be recognized that the EO coefficient depends on the hyperpolarizability β as well as the loading parameter. The magnitude of β for a chromophore is often correlated with the magnitude of μ,[9,18] which further compounds the difficulty of achieving optimum performance.

Alternative mean-field models exist, whose predictions are qualitatively similar to the Piekara model. For example, the approach of Prezhdo et al. is attractive because it is a self-consistent mean-field model.[19] To achieve a closed set of relations that determine self-consistency of the mean dipole polarization, however, the model of Prezhdo et al. replaces the local chromophore environment with a set of two interpenetrating cubic lattices whose dipoles are constrained to be in one of two states with respect to the poling field direction (an Ising-type sub-lattice). The reduction of the dipole orientations to a set of Ising-type lattices makes direct comparison of the mean field results of Prezhdo et al. with the MC simulations difficult. States exhibiting significant dipole polarization perpendicular to the poling field direction were found to be important at high density in the MC simulations (see Figure 6). The model of Prezhdo et al. also differs qualitatively from the Piekara model in that a distortion of the geometry of the sublattice used for the mean-field calculation is necessary in the former model in order to predict the decrease of the loading parameter at high density. This lattice distortion is modeled as a steric effect in the approach of Prezhdo et al. In contrast, the Piekara model is capable of predicting a decrease in the loading parameter at high density based on electrostatics alone. The MC-based calculations presented here contain only electrostatics so that the Piekara model is more appropriate for comparison with the MC results.

The MC calculations, used to model the EO parameters, were performed with point dipoles arranged on simple periodic lattices. No molecular steric effects were included so that the effects of electrostatics could be studied in isolation. MC has been applied previously to study the effects of chromophore density and dipole moment on the value of the EO loading parameter.[11] The results contained here are an investigation of the internal dipole orientation statistics of the MC calculations. The nearest-neighbor angular distribution was investigated as a function of the density, dipole moment, and temperature. The nearest-neighbor distributions that were observed in the case of a simple cubic lattice appeared to consist of a superposition of two exponentially weighted distributions. The dependence of the observed exponential distributions on the density, dipole moment, and temperature was interpreted in terms of the functional form of the local field that was posited in the analytic approach. The simple analytic theory motivated a functional form for the nature of the internal dipolar interactions, and provides insight into an interpretation of the MC numerical results. Moreover the MC results validate the dependence of the W parameter of the analytic theory on dipole moment and distances between chromophores. It is quite remarkable that such a simple relation exists. Long-range statistical order was observed in the MC calculations when the absolute orientations of the dipoles were analyzed.

As we[11] and others[20,21] have discussed, long-range order is expected in the types of systems studied here. The order, typical of nematic liquids, arises from the dipolar interactions. This long-range order is captured well by the MC calculations presented here. However, the analytic theory, because it is based

on local orientations, will not describe long-range order and therefore cannot be a complete description of the phase of the dipoles. Consequently, when the loading parameter from MC is compared with the analytic theory, the magnitude of the local field must be increased over the value expected from the nearest neighbor statistics alone. From these calculations, we are able to obtain a simple picture of dipolar forces: For the case of uniform lattices, the dipoles orient in sheets perpendicular to the direction of the poling field. Yet because the dipoles within each sheet are polarized in a direction opposite to the dipoles on neighboring sheets, the system is highly anti-ferroelectric. When the simple cubic symmetry is broken, by increasing the *XY* distance relative to *Z*, the dipoles will organize head to tail in columns. Each of these columns is highly ordered. However, in the absence of the poling field, the material is overall still anti-ferroelectric, because there are equal numbers of columns in opposing directions. The loading parameter is increased by over 2-fold when the lattice geometry is distorted tetragonally so that $A = 2$. The poling field acts to arrange the dipoles into ordered columns with a preferred columnar direction. While the fields used in the present calculations were on the order of 300 V/μM, similar enhancements in the loading parameter were also obtained with poling fields more typical of experimental conditions. The change in the loading parameter, resulting from a change in the aspect ratio of the lattice, demonstrates that if dipoles can be ordered in space to be farther apart in the *XY* plane then there will be an enhancement in the EO effect, at the same chromophore loading density. This result suggests that oblate spheroids, with a sufficiently large aspect ratio, which can be stacked with the unique spheroid axis aligned with the poling field, would improve the loading parameter and hence the EO response. Such a system would not be ferroelectric and would not spontaneously order; the system is anti-ferroelectric but would give approximately a 2-fold improvement in EO coefficient when placed in a poling field.

We have found that the lattice models predict states that are statistically anti-ferroelectric at high loading densities, for example, above 5×10^{20}/cc in Figure 8. We have not found any ferroelectric phases. This is not surprising given the conclusions of Patey,[20] who found that ferroelectric phases arise at low temperatures only when conducting boundary conditions are used in the application of Ewald sums. We employed no boundary conditions (other than standard re-entrant conditions), which is equivalent to nonconducting boundary conditions, and performed no Ewald sums. Although, in separate calculations not shown here, we found that the Ewald sums did not significantly alter our results. In a lattice model, Camp and Patey[20] considered a specific lattice, a body-centered tetragonal lattice, with an aspect ratio of 1.22. This is a slightly different lattice from the one we used in these studies. However in separate calculations, we compared simple cubic lattices to body-centered uniform lattices and found minimal differences in the order parameters as a function of loading density. Camp and Patey[20] argue that at the 1.22 aspect ratio the ferroelectric and the anti-ferroelectric phases should be of similar energy and that crossing over from one to the other can be driven by dipolar interactions alone. They obtained a ferroelectric phase by modifying the point dipole as a pair of collinear, point dipoles separated by a distance about $^1/_3$ of the lattice distance (in the *Z* direction). Thus, it may be possible for systems that are strongly anti-ferroelectric to be driven to be ferroelectric by redesigning the underlying molecules that generate the large dipoles. This may prove to be a strategy that can be added to the ordering obtained by considering oblate-shaped molecules to provide an even greater EO response.

Acknowledgment. This material is based upon work partially supported by the STC Program of the National Science Foundation No. DMR 0120967. Any opinions, findings, and conclusions or recommendations expressed in this material are those of the authors and do not necessarily reflect the views of the National Science Foundation. Support from the Air Force Office of Scientific Research is also gratefully acknowledged.

References and Notes

(1) Dalton, L. R.; Steier, W. H.; Robinson, B. H.; Zhang, C.; Ren, A.; Garner, F. S.; Chen, A.; Londergan, T.; Irwin, L.; Carlson, B.; Fifield, L.; Phelan, G.; Kincaid, C.; Amend, J.; Jen, A. K. Y. *J. Mater. Chem.* **1999**, *9*, 1905.

(2) Dalton, L. R. *Adv. Polym. Sci.* **2002**, *158*, 1.

(3) Shi, Y.; Zhang, C.; Zhang, H.; Bechtel, J.; Dalton, L. R.; Robinson, B. H.; Steier, W. H. *Science* **2000**, *288*, 119.

(4) Dalton, L. R.; Robinson, B. H.; Jen, A. K.-Y.; Steier, W. H.; Nielsen, R. D. *Opt. Mater.* **2002**, *21*, 19.

(5) Dalton, L. R. In *Electrical and Optical Polymer Sciences: Fundamentals, Methods and Applications*; Wise, D. L., Cooper, T. M., Gresser, J. D., Trantolo, D. J., Wnek, G. E., Eds.; World Scientific: Singapore, 1998; p 609.

(6) Ma, H.; Chen, B.; Takafumi, S.; Dalton, L. R.; Jen, A. K.-Y. *J. Am. Chem. Soc.* **2001**, *123*, 986.

(7) Londergan, T.; Dalton, L. R. *Mol. Cryst. Liq. Cryst.* **2000**, *353*, 211.

(8) Robinson, B. H.; Dalton, L. R.; Harper, A. W.; Ren, A.; Wang, F.; Zhang, C.; Tordova, G.; Lee, M.; Aniszfeld, R.; Garner, S. M.; Chen, A.; Steir, W. H.; Houbrecht, S.; Persoons, A.; Ledoux, P.; Zyss, J.; Jen, A. K. Y. *Chem. Phys.* **1999**, *245*, 35.

(9) Kinnibrugh, T.; Robinson, B. H.; Eichinger, B. E. *J. Phys. Chem.* **2003**, This issue.

(10) Dalton, L. R.; Harper, A. W.; Robinson, B. H. *Proc. Natl. Acad. Sci. U. S. A.* **1997**, *94*, 4842.

(11) Robinson, B. H.; Dalton, L. R. *J. Phys. Chem.* **2000**, *104*, 4785.

(12) Robinson, B. H.; Dalton, L. R. *Polym. Preprints* **2000**, *41*, 787.

(13) Piekara, A. *Proc. R. Soc. London, A* **1939**, *172*, 360.

(14) Dalton, L. R.; Robinson, B. H.; Nielsen, R.; Jen, A. K.-Y.; Steier, W. H. *Proceedings of SPIE−Int. Soc. Opt. Eng.* **2002**, *4798*, 1.

(15) Chandler, D. *Introduction to Modern Statistical Mechanics*; Oxford University Press: New York, 1987.

(16) Bottcher, C. J. F. *Theory of Electric Polarization*; Elsevier: Amsterdam, 1973.

(17) Allen, M. P.; Tildsley, D. J. *Computer Simulation of Liquids*; Oxford: Oxford, 1986.

(18) Flipse, M. C.; de Jonge, R.; Woudenberg, R. H.; Marsman, A. W.; van Walree, C. A.; Jenneskens, L. W. *Chem. Phys. Lett.* **1995**, *245*, 297.

(19) Pereverzev, Y. V.; Prezhdo, O. V. *Phys. Rev. E* **2000**, *62*, 8324.

(20) Camp, P. J.; Patey, G. N. *Phys. Rev. E* **1999**, *60*, 4280.

(21) Wei, D.; Patey, G. N. *Phys. Rev. Lett.* **1992**, *68*, 2043.